

## Electronic nature of the lock-in magnetic transition in $CeXAl_4Si_2$

J. Gunasekera,<sup>1</sup> L. Harriger,<sup>2</sup> A. Dahal,<sup>1</sup> A. Maurya,<sup>3</sup> T. Heitmann,<sup>4</sup> S. M. Disseler,<sup>2</sup> A. Thamizhavel,<sup>3</sup> S. Dhar,<sup>3</sup> D. J. Singh,<sup>1</sup> and D. K. Singh<sup>1,\*</sup>

<sup>1</sup>*Department of Physics and Astronomy, University of Missouri, Columbia, Missouri 65211, USA*

<sup>2</sup>*NIST Center for Neutron Research, Gaithersburg, Maryland 20899, USA*

<sup>3</sup>*Tata Institute of Fundamental Research, Mumbai, India*

<sup>4</sup>*University of Missouri Research Reactor, University of Missouri, Columbia, Missouri 65211, USA*

(Received 15 September 2015; revised manuscript received 11 April 2016; published 25 April 2016)

We have investigated the underlying magnetism in newly discovered single crystal Kondo lattices  $CeXAl_4Si_2$ , where  $X = Rh, Ir$ . We show that the compound undergoes an incommensurate-to-commensurate magnetic transition at  $T_c = 9.19$  K (10.75 K in Ir). The spin correlation in the incommensurate phase is described by a spin density wave configuration of Ce ions, which locks in to the long-range antiferromagnetic order at  $T = T_c$ . The analysis of the experimental data, combined with the calculation of the electronic properties, suggests the role of the Fermi surface nesting as the primary mechanism behind this phenomenon.

DOI: [10.1103/PhysRevB.93.155151](https://doi.org/10.1103/PhysRevB.93.155151)

Strongly correlated electrons systems provide a fertile research avenue that encompasses a host of electronic phenomena, such as quantum critical behavior, unconventional superconductivity, and multiferroic and unusual electronic properties associated with the reconstruction of the Fermi surface [1–7]. Among the strongly correlated electrons family, heavy electron compounds are of special interest [8–10]. Many of these materials exhibit an interplay between magnetism and unconventional superconductivity where magnetic quantum critical effect is found to play the key role [11,12]. The heuristic quantum critical phenomenon is often accompanied by a change in the Fermi surface properties [9,13]. Another unusual magnetic phenomenon, which may arise due to the change in the electronic properties in a magnetic material, is associated with the magnetic phase transition between commensurate and incommensurate order as a function of temperature; often referred to as the lock-in magnetic transition [14]. Although it is argued that the instability in the Fermi surface, causing the separation of hole and electron pockets, is the predominant mechanism, the underlying physics behind this phenomenon is a subject of debate. Similar behavior is also ascribed due to at least two other effects: (a) the distortion in the crystal structure leading to the Umklapp correction to the Landau free energy expression [15], and (b) the steplike incommensurate peaks impersonating domain walls propagation of soft solitons that merge to the commensurate wave vector via the first order phase transition (for instance, the lock-in transition in  $TaS_2$ ) [16,17].

We have performed detailed neutron scattering measurements on high quality single crystals of newly discovered Kondo lattices  $CeXAl_4Si_2$  (standard formula  $CeAl_4Si_2X$ ),  $X = Rh, Ir$ , to investigate the underlying magnetism as functions of temperature and magnetic field. We have found that both compounds undergo incommensurate-to-commensurate magnetic transition at  $T_c \simeq 9.2$  K and 10.8 K in  $X = Rh$  and Ir, respectively. The incommensurate magnetic order, which is field independent and develops below  $T_{IC} \simeq 14$  K in

$CeRhAl_4Si_2$  (16 K in  $X = Ir$ ), is given by the temperature-dependent propagation wave vector  $\mathbf{k} = (0.016, 0.016, 0.5)$  at  $T = 10$  K. The magnetic configuration in the incommensurate phase is best described by a spin density wave correlation of Ce-spins for  $9 \text{ K} \leq T \leq 14 \text{ K}$  ( $10.7 \text{ K} \leq T \leq 15.5 \text{ K}$  in  $X = Ir$ ), with Ce moments spatially fluctuating along the  $z$  axis. As the temperature is decreased below  $T \simeq 9$  K ( $T \leq 10$  K in  $X = Ir$ ), the incommensurate (IC) peaks lock-in to the long-range antiferromagnetic order via the first order magnetic transition. The analysis of neutron data, combined with previous magnetic, electrical, and heat capacity measurements on a single crystal sample [18], suggest that the lock-in magnetic transition arises due to the changes in the electronic properties of the system. Detailed calculations of the Fermi surface properties confirm that the incommensurate magnetic structure is related to the separation of electron and hole pockets in  $CeXAl_4Si_2$ .

$CeXAl_4Si_2$ , a dense Kondo lattice, crystallizes in the  $EuIrAl_4Si_2$ -type tetragonal lattice structure (space group  $P4/mmm$ ) with lattice parameters of  $a = b = 4.216 \text{ \AA}$  ( $4.221 \text{ \AA}$ ) and  $c = 7.979 \text{ \AA}$  ( $7.949 \text{ \AA}$ ) in  $X = Rh$  (Ir), as shown in the inset of Fig. 1(a). Previous magnetic and heat capacity measurements on powder and single crystal specimens suggest strong anisotropic nature of magnetic susceptibilities, with large discrepancies in Curie-Weiss temperature  $\Theta_{CW}$  for field applications along different crystallographic directions and full ordered moment values in  $CeRhAl_4Si_2$  and  $CeIrAl_4Si_2$  [18–20]. In particular, for field application along the [100] direction,  $\Theta_{CW}$  and full moment values are found to be  $-155$  K ( $-140$  K) and  $2.65 \mu_B$  ( $2.62 \mu_B$ ) in  $CeRhAl_4Si_2$  ( $X = Ir$ ), respectively [18]. Magnetic and electrical measurements in applied field on single crystal  $CeRhAl_4Si_2$  ( $X = Ir$ ) further reveal the onset of a spin-flop transition around  $H \simeq 5$  T (6.5 T), which tends to disappear at  $T \geq 10$  K [18].

Detailed neutron scattering measurements were performed on high quality single crystal samples of  $CeRhAl_4Si_2$  and  $CeIrAl_4Si_2$ , with respective masses of 0.63 g and 0.17 g, on cold triple axis spectrometer SPINS at the NIST Center for Neutron Research and on thermal triple axis spectrometer TRIAX at the Missouri University Research Reactor. Single crystal samples were synthesized using the flux growth method

\*singhdk@missouri.edu

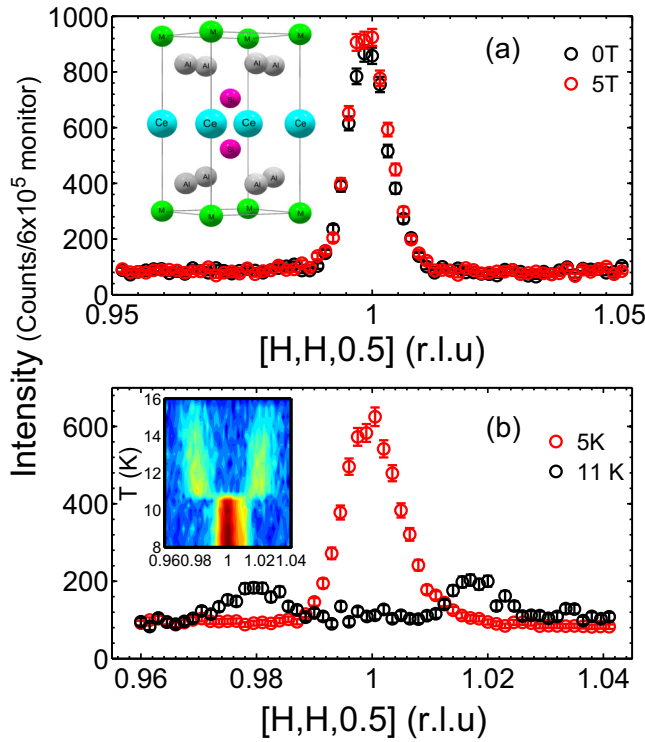


FIG. 1. Representative scans exhibiting commensurate and incommensurate magnetic reflections in  $CeXAl_4Si_2$ . (a) Elastic scan along  $[HH0.5]$  reciprocal direction, depicting commensurate magnetic reflection, at  $T = 5$  K and at different field values in  $CeRhAl_4Si_2$ . The elastic data remains unaffected to magnetic field application up to  $H = 10$  T. Similar behavior is observed in  $X = Ir$ . Inset shows the crystal structure. (b) Elastic scans along  $[HH0.5]$  direction, depicting incommensurate magnetic reflections, at  $T = 11$  K in  $CeIrAl_4Si_2$ . Similar behavior is observed in  $X = Rh$ . Inset shows the color map of incommensurate to commensurate transition as a function of temperature.

and the high quality of the samples were verified using x-ray diffraction measurements [18]. Small samples with flat geometry reduces neutron absorption cross-section, thus help us in the quantitative analysis of the neutron data. For SPINS measurements, the single crystal sample was mounted at the end of a 1 K stick and cooled in a  $^4He$  environment in a 10 T magnet. For elastic measurements, the collimator settings were M-Be filter-80'-Sample-Be filter-80'-5 blades flat analyzer detector. The measurements on TRIAX were performed using a closed cycle refrigerator with the base temperature of  $\approx 5$  K. The collimator settings for TRIAX experiment were as follows: PG filter-M-60'-Sample-PG filter-60'-flat analyzer detector. Single crystal samples were aligned in the  $[HHL]$  plane of the reciprocal space, such that the applied field direction was along  $(-110)$ .

Previous neutron scattering measurements on powder  $CeXAl_4Si_2$ ,  $X = Rh, Ir$ , were not conclusive enough to identify the magnetic correlation at intermediate temperature [19], as inferred from the susceptibility and the heat capacity measurements [18]. Unlike the powder sample, single crystal specimen allows for a much more detailed investigation of structural and magnetic properties. As shown in repre-

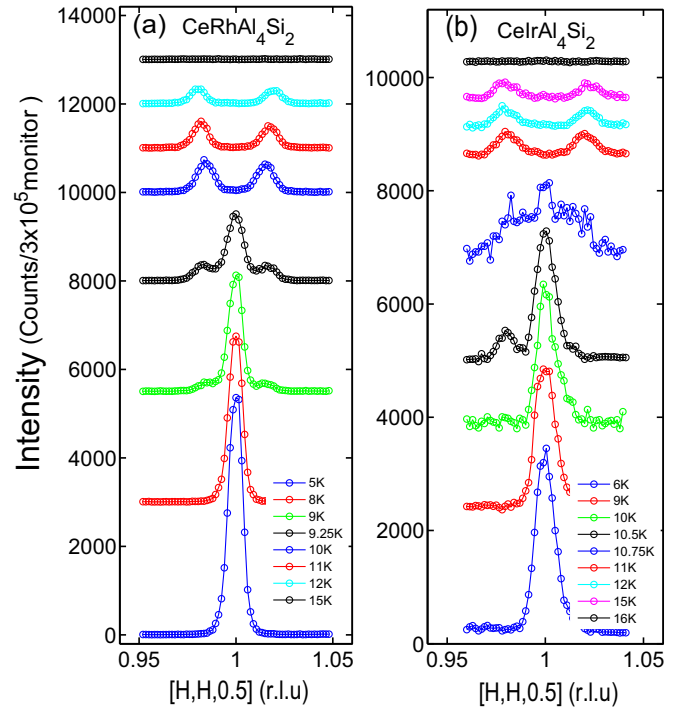


FIG. 2. Incommensurate to commensurate lock-in magnetic transition. (a) Elastic scans along  $[HH0.5]$  direction at different temperatures, exhibiting incommensurate to commensurate magnetic transition ( $T_c \approx 9.2$  K) as a function of temperature in  $CeRhAl_4Si_2$ . Experimental data are well described by a Gaussian line shape. (b) Similar behavior is observed in  $X = Ir$ , albeit the transition happens at a slightly higher temperature ( $T_c \approx 10.8$  K).

sentative Fig. 1(b), the incommensurate magnetic pattern, indicating a different magnetic structure than the collinear antiferromagnetic configuration at low temperature, develops at intermediate temperature. Since both materials crystallize in the same tetragonal structure with same ligands coordination, the observation of incommensurate magnetic pattern in both systems, albeit with different onset temperatures (as discussed below), is not a surprise.

Representative scans along the reciprocal direction  $[HH0.5]$  at different temperatures in both compounds are plotted in Figs. 2(a) and 2(b). As the measurement temperature is reduced below 14 K (16 K in  $X = Ir$ ), a pair of temperature-dependent incommensurate (IC) magnetic peaks develop with the propagation wave vector of  $\mathbf{k}_{IC} = (0.016, 0.016, 0.5)$  at  $T \approx 10$  K. The position of the IC peak, with respect to the nearest nuclear peak, is described by the wave vector:  $\mathbf{q} = \mathbf{Q} \pm \mathbf{k}$ , where  $\mathbf{Q}$  represents the nuclear peak position. As the temperature is further reduced, the incommensurate peaks first get stronger before gradually diminishing to the background level at  $T \approx 9.2$  K (10.8 K in  $X = Ir$ ). Around the same temperature, new magnetic peaks with the commensurate propagation vector  $\mathbf{k}_C = (0, 0, 0.5)$  develop in both compounds. The commensurate magnetic peaks become stronger as temperature is reduced to  $T \rightarrow 0$  K. The overall behavior is described in Figs. 3(a) and 3(b), depicting the temperature dependence of magnetic peak intensity in both commensurate and incommensurate phases. Unlike in the

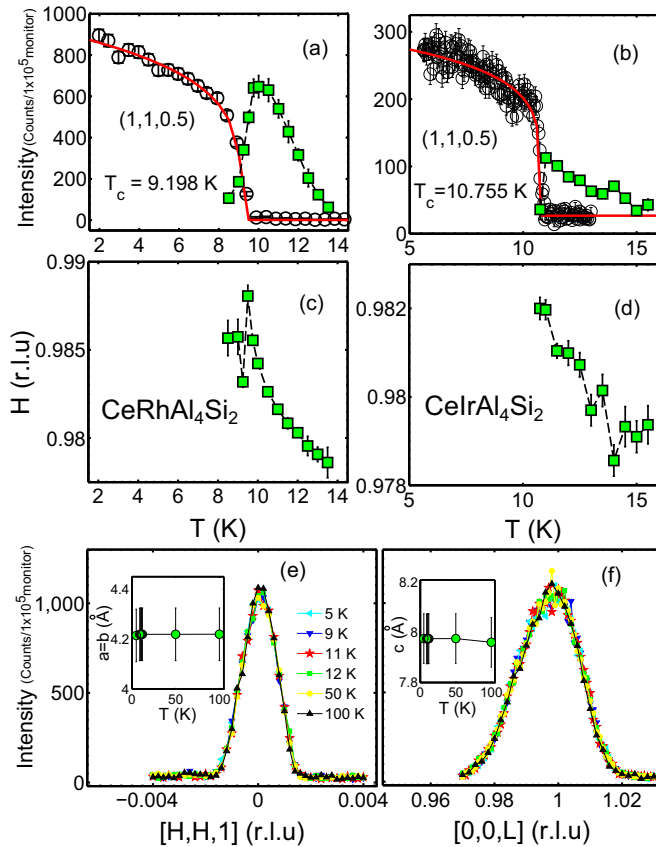


FIG. 3. Commensurate and incommensurate magnetic order parameter and movement of IC peaks. (a) and (b) Magnetic order parameters in both commensurate and incommensurate (IC) phases as a function of temperature in  $\text{CeRhAl}_4\text{Si}_2$  (a) and  $\text{CeIrAl}_4\text{Si}_2$  (b). While the IC peaks form a dome-type structure in temperature, the transition to the commensurate phase is mostly first order in nature. (c) and (d) Center of IC peak as a function of temperature, nominally at  $\mathbf{q}_{IC} = (0.98, 0.98, 0.5)$ . The IC peak moves towards the commensurate wave vector as the measurement temperature is reduced. (e) and (f) Representative scans across structural peaks as a function of temperature in  $\text{CeRhAl}_4\text{Si}_2$  (e) and  $\text{CeIrAl}_4\text{Si}_2$  (f). Clearly, no change in the position or the peak intensity of nuclear peaks are observed as the temperature is reduced through the lock-in magnetic transition.

incommensurate phase where a dome-shaped regime with the maximum intensity around  $T \simeq 10$  K (11 K in  $X = \text{Ir}$ ) occurs in temperature, the sharp temperature-dependence of the order parameter in the commensurate phase (especially in  $X = \text{Ir}$  compound) suggests a first order magnetic transition. However, elastic neutron data did not exhibit any magnetic field dependence, as shown in Fig. 1(a).

Magnetic peaks in  $\text{CeXAl}_4\text{Si}_2$ , Fig. 2, are best described by a Gaussian line shape of width limited by the instrument resolution. It indicates the presence of a long-range magnetic order in the system. In Figs. 3(c) and 3(d), we have plotted the temperature dependence of the incommensurate peak, nominally at  $\mathbf{q}_{IC} = (0.98, 0.98, 0.5)$ . As the measurement temperature is reduced, IC peak gradually moves towards the commensurate wave vector. The spectral weight shifts from IC peak to the commensurate peak in a very narrow temperature range around  $T \simeq 9$  K ( $\simeq 10.7$  K in  $X = \text{Ir}$ ), suggesting the

lock-in magnetic transition in the system [see the inset of Figs. 1(b) and 2]. In principle, this behavior can arise due to any of the three reasons: lattice distortion, soft soliton creation, or the changes in the electronic properties due to the Fermi surface reconstruction. According to the Landau-Lifshitz expression of free energy, the magnetic order parameter can transform from an incommensurate to a commensurate phase due to the Umklapp correction to the total energy [16]. The Umklapp correction is more prominent in the case of significant lattice distortion in the system, primarily causing the crystal symmetry group transformation at low temperature [21].

Measurements were performed to determine the applicability of the Umklapp correction causing an incommensurate-to-commensurate magnetic phase transition in  $\text{CeXAl}_4\text{Si}_2$ . Representative scans across structural peaks and the lattice parameters in  $\text{CeXAl}_4\text{Si}_2$  are plotted in Figs. 3(e) and 3(f). Clearly, the tetragonal lattice structure remains intact throughout the measurement; hence, rules out this possibility. Second possibility involves the creation of the soft solitons at higher temperature that merge to the commensurate wave vector via the first order transition as the measurement temperature is reduced [16,17]. Soft solitons are accompanied by a steplike function of incommensurate (IC) reflections of higher harmonics. Also, the IC peaks get closer to each other as temperature is reduced.  $\text{CeXAl}_4\text{Si}_2$  exhibits at least two characteristics of solitons: a first order-type magnetic transition to the commensurate phase (more prominently in  $X = \text{Ir}$ ) and the temperature-dependent movement of IC peaks towards the commensurate wave vector. However, no evidence of the steplike function of higher harmonic IC peaks were observed in neutron scattering measurements.

Next, we discuss the nature of long-range magnetic correlation in  $\text{CeXAl}_4\text{Si}_2$ . The incommensurate magnetic reflections are usually associated to the long-range magnetic order of a density wave or the square wave pattern. Measurements were performed to higher order Brillouin zones (BZ) at two temperatures,  $T = 5$  K and 10 K, to understand the nature of magnetic correlations. At low temperature, magnetic peak intensities across the extended BZ is best described by an antiferromagnetic spin correlation with Ce spins pointing along the  $z$  axis, see the inset of Fig. 4(a). The ordered moment of correlated Ce ions is found to be  $1.24(0.17) \mu_B$  and  $1.44(0.16) \mu_B$  in  $X = \text{Rh}$  and  $\text{Ir}$ , respectively. This is also consistent with a previous report of neutron scattering measurements on powder  $\text{CeXAl}_4\text{Si}_2$  [19]. In order to determine the spin correlation associated to IC peaks at relatively higher temperature ( $T \simeq 10$  K), numerical modeling of the experimental data was performed using the following expression for the ordered moment  $\mathbf{S}_{ij}$  [22,23]:

$$\mathbf{S}_{ij} = \mathbf{A}_i \cos(\mathbf{k} \cdot \mathbf{r}_j + \psi_j) + \mathbf{B}_i \sin(\mathbf{k} \cdot \mathbf{r}_j + \psi_j), \quad (1)$$

where  $\mathbf{S}_{ij}$  is the moment of the  $i$ th ion in the  $j$ th unit cell and  $\mathbf{k}$  is the propagation wave vector of the spin density wave [23]. The magnetic peaks were normalized to the intensities of the nuclear peaks, after resolution corrections, and the spin structure was determined using the above formula. The numerical modeling also involved averaging the magnetic structure factor over four equally populated domains. Magnetic structure in the IC phase is best described by a spin density wave (SDW) configuration of propagation vector  $\mathbf{k} = (0.016, 0.016, 0.5)$ .

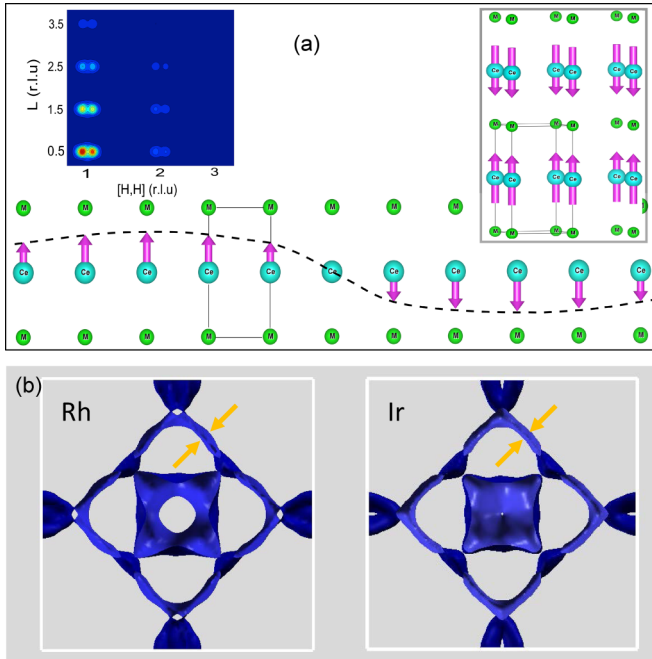


FIG. 4. (Top panel) Top left panel manifests the simulated magnetic pattern in the incommensurate phase, which is consistent with the experimental data. Top right inset shows the spin correlation of Ce ions in the commensurate phase. While the commensurate phase is described by the antiferromagnetic correlation of Ce ions along the  $z$  axis, the incommensurate structure (as shown in lower panel) is best described by a spin density wave with Ce spins spatially fluctuating along the  $z$  axis. (Bottom panel)  $c$ -axis view of hole Fermi surfaces of  $\text{LaRhAl}_4\text{Si}_2$  and  $\text{LaIrAl}_4\text{Si}_2$  with the nesting vector of the shell-like section indicated by the orange arrows. Almost identical nesting vector is obtained in the Ce analogs (see Supplemental Material for details). The propagation wave vector, as inferred from neutron scattering measurements, is similar to the calculated nesting vector.

The SDW state in the IC region is the only state allowed by the symmetry under the representational analysis. It was confirmed by magnetic structure refinement using the FullProf suite. The spin correlation of Ce spins, spatially fluctuating along the  $z$  axis, is shown in Fig. 4(a). The ordered moment associated to the SDW configuration is found to be  $0.42(0.12) \mu_B$  and  $0.69(0.16) \mu_B$  in  $X = \text{Rh}$  and  $\text{Ir}$ , respectively. The ordered moment values, in both the commensurate and the incommensurate phases, are much smaller than full moment values in respective compounds. The smaller value of the

ordered moment possibly illustrates strong Kondo screening of the localized moment by surrounding conduction electrons in these dense Kondo lattice systems. It is one possibility, in addition to other mechanisms that are not clear.

To verify the electronic nature of the incommensurate structure, calculations were performed for  $\text{CeRhAl}_4\text{Si}_2$  and  $\text{CeIrAl}_4\text{Si}_2$  and the La analogues with the same crystal structures using the generalized gradient approximation of Perdew, Burke, and Ernzerhof (PBE) and with the GGA+ $U$  method (PBE+ $U$ ) (see Supplemental Material for details) [24,25]. We find that the C-AFM structure is lower in energy than the ferromagnetic ordering for both compounds regardless of whether the Coulomb repulsion  $U$  was included. The Fermi surfaces for the C-AFM structure are shown in Fig. S3 of the Supplemental Material. They show the effect of zone folding along the  $k_z$  direction, but otherwise retain the sheets seen in the La analogues. The fact that the Fermi surface is not gapped by the ordering indicates a superexchange mechanism for the C-AFM ordering. Importantly, the metallic character and the shell-like structure of the hole sheets around the zone edges is retained. This shell structure implies a low- $q$  nesting in the  $\langle 110 \rangle$  direction [Fig. 4(b)], consistent with the observed incommensurate ground state structure.

In summary, we have performed detailed experimental investigation of the underlying magnetism and associated lock-in magnetic transition in single crystals  $\text{CeXAl}_4\text{Si}_2$ . Both compounds exhibit sharp magnetic transition from an incommensurate phase, at intermediate temperatures, to the commensurate phase at low temperatures. The spin structures in commensurate and incommensurate phases are manifested by long-range antiferromagnetic and spin density wave configurations of correlated Ce ions, respectively. The analysis of the experimental data, combined with the calculation of the Fermi surfaces, suggests that the incommensurate phase can be arising due to the Fermi surfaces nesting. Although this is the most plausible explanation of the incommensurate phase transition, a possible role of the soliton propagation in the lock-in phase transition cannot be completely ruled out (as discussed previously). Future experiments, including detailed inelastic neutron scattering measurements on bigger samples, will be helpful in further understanding the role of possible soliton propagation in these newly discovered Kondo lattices [16].

Authors acknowledge the support provided by the Department of Commerce facility NIST Center for Neutron Research. Authors are thankful to J. Leo and A. Ye for help with the neutron scattering experiments.

- [1] C. M. Varma, *Rev. Mod. Phys.* **48**, 219 (1976).
- [2] S. Sachdev, *Quantum phase transitions*. (Cambridge University Press, New York, 1999).
- [3] Z. Fisk, D. Hess, C. Pethick, D. Pines, J. Smith, J. Thomson, and J. Willis, *Science* **239**, 33 (1988)
- [4] S. S. Saxena, P. Agarwal, K. Ahilan, F. M. Grosche, R. K. W. Haselwimmer, M. J. Steiner, E. Pugh, I. R. Walker, S. R. Julian, P. Monthoux, G. G. Lonzarich, A. Huxley, I. Sheikin,

D. Braithwaite, and J. Flouquet, *Nature (London)* **406**, 587 (2000).

- [5] W. Eerenstein, N. D. Mathur, and J. F. Scott, *Nature (London)* **442**, 759 (2006).
- [6] L. S. Wu, M. S. Kim, K. Park, A. M. Tsvetlik, and M. C. Aronson, *Proc. Natl. Acad. Sci.* **111**, 14088 (2014).
- [7] H. Watanabe and M. Ogata, *J. Phys.: Conf. Ser.* **150**, 042227 (2009).

- [8] G. R. Stewart, *Rev. Mod. Phys.* **56**, 755 (1984).
- [9] Q. Si, S. Rabello, K. Ingersent, and J. L. Smith, *Nature (London)* **413**, 804 (2001).
- [10] P. Coleman, C. Ppin, Q. Si and R. Ramazashvili, *J. Phys.: Condens. Matter* **13**, R723 (2001).
- [11] D. M. Broun, *Nat. Phys.* **4**, 170 (2008).
- [12] A. Schroder, G. Aeppli, R. Coldea, M. Adams, O. Stockert, H. v. Lhneysen, E. Bucher, R. Ramazashvili, and P. Coleman, *Nature (London)* **407**, 351 (2000).
- [13] P. Gegenwart, Q. Si, and F. Steglich, *Nat. Phys.* **4**, 186 (2008).
- [14] E. Fawcett, *Rev. Mod. Phys.* **60**, 209 (1988).
- [15] G. C. Milward, M. J. Caldern and P. B. Littlewood, *Nature (London)* **433**, 607 (2005).
- [16] R. A. Cowley, *Adv. Phys.* **29**, 1 (1980).
- [17] D. E. Moncton, J. D. Axe, and F. J. DiSalvo, *Phys. Rev. Lett.* **34**, 734 (1975).
- [18] A. Maurya, R. Kulkarni, A. Thamizhavel, D. Paudyal, and S. K. Dhar, *J. Phys. Soc. Jpn.* **85**, 034720 (2016).
- [19] N. J. Ghimire, S. Calder, M. Janoschek, and E. D. Bauer, *J. Phys.: Cond. Matt.* **27**, 245603 (2015).
- [20] N. J. Ghimire, F. Ronning, D. J. Williams, B. L. Scott, Y. Luo, J. D. Thomson, and E. D. Bauer, *J. Phys.: Cond. Matt.* **27**, 025601 (2015).
- [21] P. Manuel, L. C. Chapon, I. S. Todorov, D. Y. Chung, J.-P. Castellan, S. Rosenkranz, R. Osborn, P. Toledano, and M. G. Kanatzidis, *Phys. Rev. B* **81**, 184402 (2010).
- [22] W. Bao, P. G. Pagliuso, J. L. Sarrao, J. D. Thompson, Z. Fisk, J. W. Lynn, and R. W. Erwin, *Phys. Rev. B* **62**, R14621 (2000).
- [23] O. Zaharko, A. Daoud-Aladine, S. Streule, J. Mesot, P.-J. Brown, and H. Berger, *Phys. Rev. Lett.* **93**, 217206 (2004).
- [24] See Supplemental Material at <http://link.aps.org/supplemental/10.1103/PhysRevB.93.155151> for detailed calculations of the band structure properties of CeXAl<sub>4</sub>Si<sub>2</sub>.
- [25] J. P. Perdew, K. Burke, and M. Ernzerhof, *Phys. Rev. Lett.* **77**, 3865 (1996).